ER-associated retrograde SNAREs and the Dsl1 complex mediate an alternative, Sey1p-independent homotypic ER fusion pathway

Jason V. Rogers[a,*], Conor McMahon[a,*], Anastasia Baryshnikova[b], Frederick M. Hughson[a], and Mark D. Rose[a]

[a]Department of Molecular Biology and [b]Lewis-Sigler Institute for Integrative Genomics, Princeton University, Princeton, NJ 08544-1014

ABSTRACT **The peripheral endoplasmic reticulum (ER) network is dynamically maintained by homotypic (ER–ER) fusion. In *Saccharomyces cerevisiae*, the dynamin-like GTPase Sey1p can mediate ER–ER fusion, but *sey1*Δ cells have no growth defect and only slightly perturbed ER structure. Recent work suggested that ER-localized soluble *N*-ethylmaleimide–sensitive factor attachment protein receptors (SNAREs) mediate a Sey1p-independent ER–ER fusion pathway. However, an alternative explanation—that the observed phenotypes arose from perturbed vesicle trafficking—could not be ruled out. In this study, we used candidate and synthetic genetic array (SGA) approaches to more fully characterize SNARE-mediated ER–ER fusion. We found that Dsl1 complex mutations in *sey1*Δ cells cause strong synthetic growth and ER structure defects and delayed ER–ER fusion in vivo, additionally implicating the Dsl1 complex in SNARE-mediated ER–ER fusion. In contrast, cytosolic coat protein I (COPI) vesicle coat mutations in *sey1*Δ cells caused no synthetic defects, excluding perturbed retrograde trafficking as a cause for the previously observed synthetic defects. Finally, deleting the reticulons that help maintain ER architecture in cells disrupted for both ER–ER fusion pathways caused almost complete inviability. We conclude that the ER SNAREs and the Dsl1 complex directly mediate Sey1p-independent ER–ER fusion and that, in the absence of both pathways, cell viability depends upon membrane curvature–promoting reticulons.**

Monitoring Editor
Anne Spang
University of Basel

Received: Jul 16, 2014
Revised: Aug 26, 2014
Accepted: Aug 28, 2014

INTRODUCTION

In all eukaryotes, the endoplasmic reticulum (ER) consists of a branched network of tubules and ribosome-dense sheets (cisternae) that is continuous with the outer nuclear envelope. In *Saccharomyces cerevisiae*, the majority of the ER network resides at the cell cortex along the plasma membrane (peripheral ER), with several tubules connecting to the outer nuclear envelope (nuclear ER). Functionally, the ER mediates multiple processes, including protein synthesis and secretion, lipid synthesis, and calcium regulation (reviewed in Schuldiner and Weissman, 2013). Recent research has identified contact sites between the ER and most other organelles, implicating the ER in additional processes, including lipid droplet biogenesis, lipid transfer, and mitochondrial division (reviewed in English and Voeltz, 2013).

ER tubules are shaped and maintained by the reticulons (Rtn1p and Rtn2p in yeast) and the reticulon-like protein Yop1p (Voeltz *et al.*, 2006; reviewed in Chen *et al.*, 2013). Rtn1p or Yop1p is sufficient to form tubules in proteoliposomes in vitro (Hu *et al.*, 2008) and likely functions by forming a curvature-inducing wedge in the lipid bilayer (Voeltz *et al.*, 2006; Shibata *et al.*, 2008; Zurek *et al.*, 2011). Simultaneous deletion of *rtn1*, *rtn2*, and *yop1* results in an almost entirely cisternal, nontubulated peripheral ER (West *et al.*, 2011). Surprisingly, however, this triple mutant displays only a minor growth defect (Voeltz *et al.*, 2006; Chen *et al.*, 2012).

Over time, the ER network must alter its structure dynamically, while maintaining lumenal continuity, by forming new branch points or by merging existing branches at three-way tubule junctions via

This article was published online ahead of print in MBoC in Press (http://www.molbiolcell.org/cgi/doi/10.1091/mbc.E14-07-1220) on September 3, 2014.

*These authors contributed equally to this work.

Address correspondence to: Mark D. Rose (mdrose@princeton.edu).

Abbreviations used: CATCHR, complex associated with tethering containing helical rods; COPI, cytosolic coat protein I; ER, endoplasmic reticulum; GFP, green fluorescent protein; ORF, open reading frame; PBS, phosphate-buffered saline; SGA, synthetic genetic array; SM, Sec1/Munc18; SNARE, soluble *N*-ethylmaleimide–sensitive factor attachment protein receptor; YEPD, yeast extract/peptone/dextrose.

homotypic (ER–ER) fusion (Lee and Chen, 1988). Homotypic ER fusion is mediated in mammals by the dynamin-like GTPase atlastin and in yeast by its functional orthologue Sey1p (Hu *et al.*, 2009; Orso *et al.*, 2009). Sey1p is enriched at three-way junctions in the peripheral ER and binds to the reticulons Rtn1p and Yop1p (Hu *et al.*, 2009). Surprisingly, *sey1*Δ mutants have no growth defect and relatively normal ER structure, similar to *rtn1*Δ and *yop1*Δ single mutants. *sey1*Δ *rtn1*Δ and *sey1*Δ *yop1*Δ double mutants, however, display abnormal, nontubulated peripheral ER with enlarged cisternae (Hu *et al.*, 2009). Despite the lack of a strong growth or structural defect, *sey1*Δ mutants exhibit a decreased (but not abolished) rate of homotypic ER fusion in vivo, whereas *rtn1*Δ *rtn2*Δ *yop1*Δ mutants, which have extremely perturbed ER structure, exhibit a wild-type homotypic ER fusion rate (Anwar *et al.*, 2012). Consistent with a direct role in ER–ER fusion, Sey1p is sufficient to mediate proteoliposome fusion in vitro (Anwar *et al.*, 2012). Another protein, Lnp1p, also resides at three-way tubule junctions and appears to antagonize Sey1p fusogenic activity, possibly by promoting ring closure (Chen *et al.*, 2012).

Together these findings demonstrate that Sey1p mediates homotypic ER fusion, but the relatively weak *sey1*Δ phenotypes suggest there is a second, partially redundant, Sey1p-independent homotypic ER fusion pathway. Patel *et al.* (1998) demonstrated that ER membranes isolated from *ufe1-1* cells were defective in an in vitro ER–ER fusion assay. More recently, strong synthetic growth and ER structure defects were demonstrated for double mutants of *sey1*Δ and the three ER-bound retrograde (Golgi-to-ER) SNAREs (soluble *N*-ethylmaleimide–sensitive factor attachment protein receptors) *sec20*, *ufe1*, and *use1* (Anwar *et al.*, 2012; Rogers *et al.*, 2013). Moreover, *sey1*Δ *ufe1-1* double mutants had an even slower rate of homotypic ER fusion than *sey1*Δ or *ufe1-1* single mutants (Anwar *et al.*, 2012). These data suggest that SNARE proteins mediate the hypothesized Sey1p-independent homotypic ER fusion pathway.

SNAREs mediate vesicle fusion during cargo trafficking between organelles (reviewed in Delic *et al.*, 2013). To fuse vesicles, SNARE proteins on the incoming vesicle bind to SNAREs on the target membrane and form a four-helix coiled-coil SNARE complex that forces the lipid membranes into close apposition (Sutton *et al.*, 1998). In vivo, unique sets of SNARE proteins (usually four SNAREs) mediate the different vesicle-trafficking steps, although some SNAREs are used in multiple pathways (Burri and Lithgow, 2004).

Although SNAREs are sufficient to fuse vesicles in vitro (Weber *et al.*, 1998), vesicle trafficking in vivo additionally requires vesicle coats, Rab GTPases, and SM (Sec1/Munc18) proteins, and tethering complexes (reviewed in Hong and Lev, 2014). In retrograde vesicle trafficking, the v-SNARE Sec22p on *cis*-Golgi–derived cytosolic coat protein I (COPI)-coated vesicles binds the t-SNAREs Sec20p, Ufe1p, and Use1p on the ER to catalyze vesicle–ER fusion (reviewed in Spang, 2013). Retrograde trafficking additionally requires the Rab GTPase Ypt1p, the SM protein Sly1p, and the Dsl1 tethering complex (Ossig *et al.*, 1991; Jedd *et al.*, 1995; Kraynack *et al.*, 2005; Li *et al.*, 2005; Kamena *et al.*, 2008). The Dsl1 tethering complex is a CATCHR (complex associated with tethering containing helical rods) family member comprising the subunits Tip20p, Dsl1p, and Sec39p/Dsl3. This complex is thought to mediate the initial connection between the ER membrane and an incoming vesicle. Specifically, the Dsl1 complex is anchored to the ER membrane through interactions of two of its subunits (Tip20p and Sec39p) with two ER t-SNAREs (Sec20p and Use1p; Figure 1A; Andag *et al.*, 2001; Andag and Schmitt, 2003; Ren *et al.*, 2009; Tripathi *et al.*, 2009; Zink *et al.*, 2009). The third Dsl1 complex subunit, Dsl1p, connects Tip20p to Sec39p and contains a flexible 80-residue segment called the "lasso." The lasso, located at the tip of the 20-nm-tall Dsl1 complex, binds two subunits of COPI coats, α-COP (Cop1p) and δ-COP (Ret2p). By binding multiple ER SNAREs and tethering the incoming vesicle near the ER membrane, the Dsl1 complex appears to promote the assembly of productive *trans*-SNARE complexes; it may also facilitate vesicle uncoating (Ren *et al.*, 2009; Zink *et al.*, 2009; Diefenbacher *et al.*, 2011).

Although it appeared from previous work (Anwar *et al.*, 2012; Rogers *et al.*, 2013) that the retrograde SNAREs Sec20p, Ufe1p, and Use1p mediate a redundant, Sey1p-independent homotypic ER

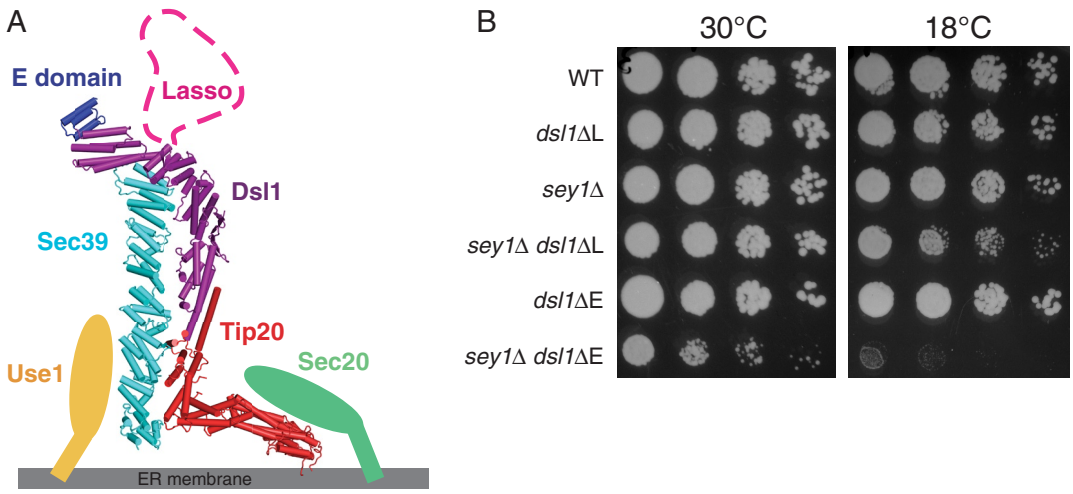

FIGURE 1: SNARE-mediated homotypic ER fusion requires *DSL1*. (A) The Dsl1 complex (Dsl1p-Sec39p-Tip20p) binds to the N-terminal regulatory domains of the SNAREs Use1p and Sec20p through interactions with Sec39p and Tip20p, respectively. The flexible lasso domain of Dsl1p binds to the COPI coatomer (not shown; adapted from Ren *et al.*, 2009). (B) Growth assays (see *Materials and Methods*) of wild type (MY14008), *dsl1*ΔL (MY14012), *sey1*Δ (MY14016), *sey1*Δ *dsl1*ΔL (MY14020), *dsl1*ΔE (MY14024), and *sey1*Δ *dsl1*ΔE (MY14028), grown on YEPD for 2 d at 30°C or 6 d at 18°C. Each spot from left to right represents a 10-fold dilution.

fusion pathway, several fundamental questions remained. First, it is possible that the synthetic growth and ER structure defects are due to downstream effects of perturbed retrograde vesicle trafficking. Second, it is unclear whether the SNAREs act in isolation or in combination with their normal vesicle-trafficking accessory proteins, including the Dsl1 tethering complex and the COPI coat. Third, it remained possible that the Sey1p-mediated and putative SNARE-mediated homotypic ER fusion pathways are not truly redundant but might mediate distinct subsets of homotypic ER fusion events. In this study, we have further characterized SNARE-mediated homotypic ER fusion and determined that it requires the Dsl1 complex but not the COPI coat, is not a result of perturbed retrograde vesicle trafficking, and is only partially redundant with Sey1p-mediated homotypic ER fusion.

RESULTS

SNARE-mediated homotypic ER fusion requires *DSL1*

Cells containing both a *sey1* deletion and a mutant retrograde SNARE allele (*sec20-1*, *ufe1-1*, *use1-10AA*, or *use1-0layer*) have strong synthetic growth and ER structural defects not seen in either single mutant (Anwar *et al.*, 2012; Rogers *et al.*, 2013). We hypothesized that homotypic ER fusion is mediated by two parallel pathways, one Sey1p mediated and the other SNARE mediated, and that only disruption of both pathways results in severe ER–ER fusion and growth defects.

To assess whether the SNAREs act with their normal accessory proteins or alone, we first created *sey1*Δ *dsl1* double mutants and assayed possible synthetic growth defects. Dsl1p, like the other subunits of the Dsl1 complex, Tip20p and Sec39p/Dsl3p, is encoded by an essential gene. We assayed two *dsl1* mutants in this study: *dsl1*ΔE and *dsl1*ΔL (Figure 1A). The C-terminal E domain is the most highly conserved region of Dsl1p (Zink *et al.*, 2009), while the flexible L (lasso) region mediates α-COP (Cop1p)- and δ-COP (Ret2p) binding (Andag *et al.*, 2001; Andag and Schmitt, 2003; Zink *et al.*, 2009); remarkably, neither the E domain nor the lasso is needed in vivo for normal growth (Zink *et al.*, 2009; R. W. Baker and F. M. H., unpublished data). Interestingly, *sey1*Δ *dsl1*ΔE double mutants exhibited a strong synthetic growth defect at 30°C and an even more severe defect at 18°C, whereas *sey1*Δ *dsl1*ΔL mutants exhibited no growth defect at 30°C and a minor growth defect at 18°C (Figure 1B). These data suggest that SNARE-mediated ER–ER fusion requires Dsl1p but not the COPI-binding lasso.

SNARE-mediated homotypic ER fusion requires the entire Dsl1 complex but not the COPI coat

Because *dsl1*ΔE but not *dsl1*ΔL mutants exhibited synthetic growth defects with *sey1*Δ, we screened for additional genetic interactions to gain insight into the function of the Dsl1p E domain. Additionally, we reasoned that this screen might identify novel components of the Sey1p-mediated ER–ER fusion pathway, as any pathway-specific components should, like *sey1*Δ, display negative genetic interactions with *dsl1*ΔE but not with *dsl1*ΔL. To perform the screen, we used synthetic genetic array (SGA) technology. We crossed each strain to a genome-wide set of nonessential deletion mutants (~4300 gene deletion strains) and a large-scale temperature-sensitive mutant collection (~1200 temperature-sensitive strains). We assessed the growth of double-mutant haploids isolated from these crosses using previously published methodology (Baryshnikova *et al.*, 2010; Costanzo *et al.*, 2010). Briefly, we assigned each double mutant an SGA score based on colony size measurements and a multiplicative fitness model. A negative SGA score indicates that the double mutant grew more poorly than expected (synthetic growth defect), whereas a positive score indicates more robust growth than expected.

To identify the most informative genetic interactions, we grouped the interactions into three classes: interactions shared between *dsl1*ΔE and *dsl1*ΔL, *dsl1*ΔL-specific interactions, and *dsl1*ΔE-specific interactions (Figure 2A; full data set available in Supplemental Table S1; classes determined via a cutoff score and a difference threshold; see *Materials and Methods*). As expected, the strongest interactions shared between *dsl1*ΔE and *dsl1*ΔL consisted of known components of vesicle trafficking. In the *dsl1*ΔL-specific class, we identified five negative interactions: *pse1-41*, *hir1*Δ, *mps3-1*, *chk1*Δ, and *cse2*Δ. Four of these genes have nuclear roles: Pse1p interacts with nuclear pore complexes, Mps3p resides at the half-bridge and mediates spindle pole body formation, Hir1p is a subunit of the histone regulation complex, and Cse2p is a subunit of the RNA polymerase II mediator complex. Interestingly, while *pse1-41* is by far the strongest *dsl1*ΔL-specific negative genetic interaction, *pse1-34* is among the strongest *dsl1*ΔL-specific positive interactions. The final interaction, *chk1*Δ, uniquely interacts both negatively with *dsl1*ΔL and positively with *dsl1*ΔE. Chk1p is a checkpoint kinase that mediates cell cycle arrest.

Among the 22 *dsl1*ΔE-specific negative interactions (Table 1), eight were related to trafficking (although not exclusively retrograde trafficking), and seven were related to transcriptional regulation. The final seven interactions consist of *sey1*Δ, whose *dsl1*ΔE-specific negative interaction (Figure 1B) motivated the genome-wide screen; *ice2*Δ, a gene involved in inheritance of cortical ER (Estrada de Martin *et al.*, 2005) that also has a negative genetic interaction with *sey1*Δ (Figure 2B); *act1-2*, an actin allele; *pyc2*Δ, a pyruvate carboxylase isoform; *atg15*Δ, a lipase involved in autophagy; and two dubious open reading frames (ORFs), *ygr139w*Δ and *ypr050c*Δ. Of note, although *act1-2* displayed the strongest negative genetic interaction, 19 other *act1* alleles tested displayed no genetic interaction. Allele-specific genetic interactions often result from physical interactions (Sandrock *et al.*, 1997), raising the possibility that Dsl1p and Act1p interact physically, although it also possible that *act1-2* specifically disrupts Sey1p-mediated ER–ER fusion. It is possible that any of the aforementioned *DSL1*-interacting genes could be new members of the Sey1p-mediated ER–ER fusion pathway; however, we have not yet studied these genes further.

Following similar logic, we reasoned that any additional components in the SNARE/Dsl1-mediated ER–ER fusion pathway should, like *dsl1*ΔE, display negative genetic interactions with *sey1*Δ. Therefore we examined independently generated *sey1*Δ SGA data (Costanzo *et al.*, 2010; unpublished data [version 13-04-22], C. Boone, University of Toronto). As expected, the strongest negative synthetic genetic interactions with *sey1*Δ include *use1*-TS (temperature sensitive), a retrograde SNARE implicated previously in SNARE-mediated ER–ER fusion; *sec39-1*, a Dsl1 complex subunit; and *sly1*-TS, an SM protein required for normal retrograde trafficking (Table 2, interactions with SGA score ≤ −0.25). These results suggest that SNARE-mediated homotypic ER fusion may require the SM protein Sly1p and possibly the entire Dsl1 complex. We discuss the potential role of the remaining five *sey1*Δ interactions in the *Discussion*.

Notably, we also observed that *sey1*Δ exhibited no genetic interactions with the members of the COPI coat (*cop1-1*, *ret2-1*, *ret3-1*, *sec21-1*, *sec26*$_{F856A,W860A}$, *sec26-2*, *sec27-1*, and *sec28*Δ), whereas both *dsl1*ΔL and *dsl1*ΔE exhibited strong interactions with most members (Figure 2B). Additionally, with the exception of *sec23-1*, other nonretrograde vesicle-trafficking pathway components showed no synthetic interactions with *sey1*Δ (see Table S1 for a listing of SGA data available for vesicle-trafficking components).

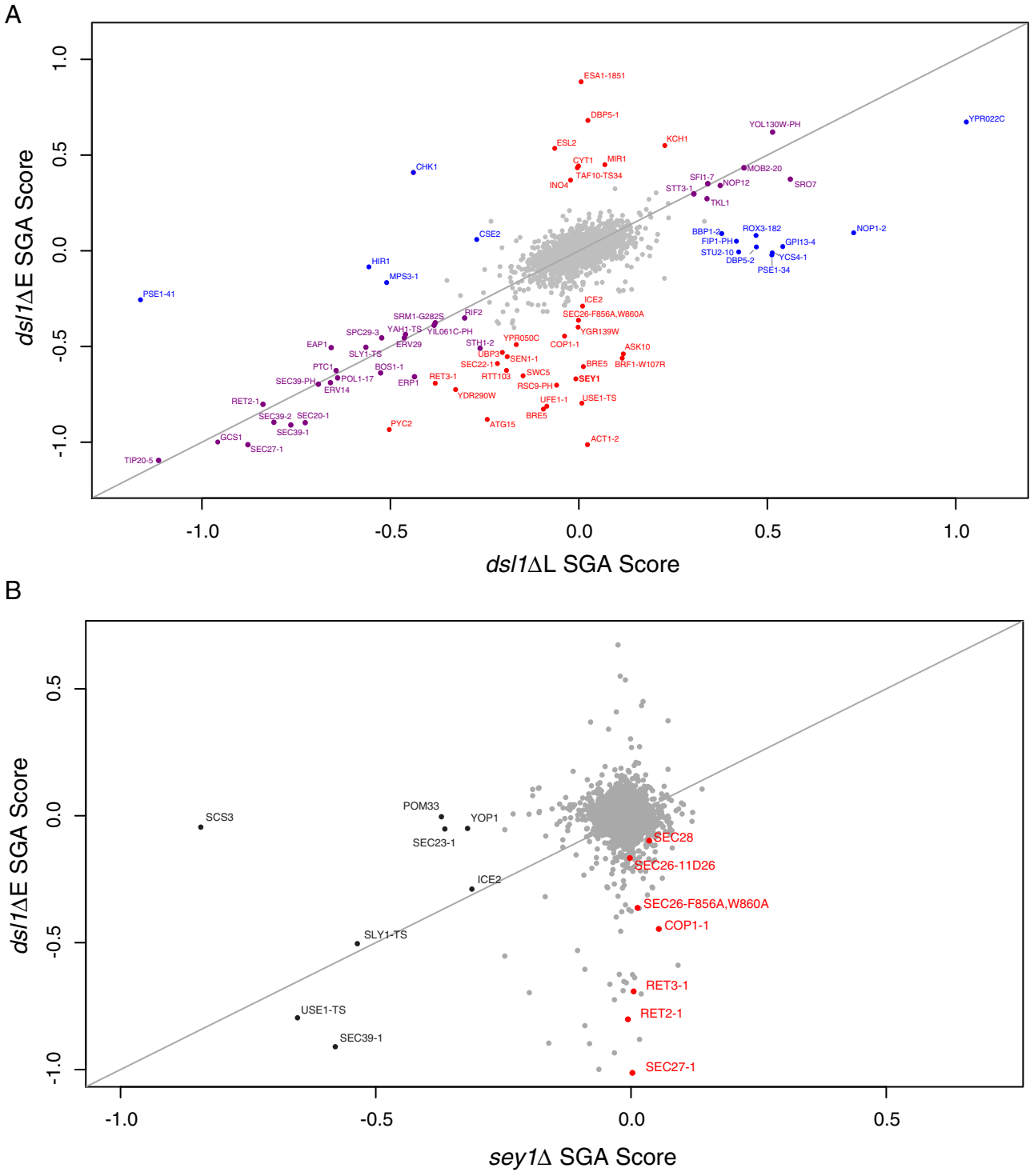

FIGURE 2: *DSL1* and *SEY1* SGAs. (A) Scatterplot of the SGA scores between *dsl1*ΔL, *dsl1*ΔE, and the indicated alleles. Genes without an allele designation are deletions. Identical scores would fall on the diagonal line. Alleles listed in purple have similar scores for both Dsl1 alleles (see *Materials and Methods* for classification metric), alleles listed in blue are classified as *dsl1*ΔL-specific, and alleles listed in red are classified as *dsl1*ΔE-specific. A few genes were tested multiple times independently during the SGA experiment (e.g., *bre5*Δ) and therefore appear multiple times in the scatterplot. (B) As in A, except *dsl1*ΔE is compared with independently derived *sey1*Δ SGA data (Costanzo *et al.*, 2010; unpublished data [version 13-04-22], Boone lab). Only alleles with data present for both *dsl1*ΔE and *sey1*Δ are plotted. Alleles of genes encoding subunits of the COPI coat complex are shown in red. The strongest *sey1*Δ-interacting alleles are shown in black.

Therefore it is unlikely that the observed genetic interactions between *sey1*Δ and the SNAREs, *dsl1*ΔE, and *sec39-1* are simply a downstream result of perturbed vesicle trafficking. Instead, our data suggest that the SNAREs and the Dsl1 complex together directly mediate Sey1p-independent ER–ER fusion, whereas the COPI coat functions specifically in retrograde vesicle trafficking.

Allele	*dsl1*ΔE	*dsl1*ΔL	Description
Vesicular traffic			
*bre5*Δ	–0.83	–0.09	Ubiquitin protease cofactor; regulates anterograde/retrograde transport
ufe1-1	–0.81	–0.09	ER-localized SNARE required for retrograde vesicular traffic
use1-TS	–0.80	0.01	ER-localized SNARE required for retrograde vesicular traffic
ret3-1	–0.69	–0.38	Zeta subunit of the COPI vesicle coatomer complex
sec22-1	–0.59	–0.22	SNARE required for retrograde and anterograde vesicular traffic
*ubp3*Δ	–0.53	–0.20	Ubiquitin-specific protease involved in transport and osmotic response
cop1-1	–0.45	–0.04	Alpha subunit of COPI vesicle coatomer complex
sec26-F856A,W860A	–0.36	0.00	Beta subunit of COPI vesicle coatomer complex
Transcription			
*ydr290W*Δ	–0.73	–0.33	ORF overlaps *RTT103*
rsc9-PH	–0.70	–0.06	Component of the RSC chromatin remodeling complex
*swc5*Δ	–0.65	–0.15	Component of the SWR1 chromatin remodeling complex
*rtt103*Δ	–0.63	–0.19	Protein involved in transcription termination by RNA polymerase II
brf1-W107R	–0.56	0.12	RNA polymerase III transcription initiation factor TFIIIB B–related factor
sen1-1	–0.55	–0.19	Presumed helicase and subunit of the Nrd1 complex
*ask10*Δ	–0.54	0.12	Component of RNA polymerase II holoenzyme
Other			
act1-2	–1.01	0.02	Actin
*pyc2*Δ	–0.93	–0.50	Pyruvate carboxylase isoform
*atg15*Δ	–0.88	–0.24	Lipase required for intravacuolar lysis of autophagic and Cvt bodies
*sey1*Δ	–0.67	–0.01	Dynamin-like GTPase that mediates homotypic ER fusion
*ypr050C*Δ	–0.49	–0.17	Dubious ORF
*ygr139W*Δ	–0.40	0.00	Dubious ORF
*ice2*Δ	–0.29	0.01	Integral ER membrane protein with type-III transmembrane domains

Class specificity as in Figure 2A, determined via cutoff score (–0.25) and difference threshold (0.25); see *Materials and Methods* for full classification metric.

TABLE 1: SGA scores of *dsl1*ΔE-specific negative genetic interactions, grouped by known functions.

We manually verified the most important SGA results and checked for synthetic growth defects between *sey1*Δ and candidates that were missing from the SGA arrays. We confirmed the synthetic growth defect in *sey1*Δ *sec39-1* mutants (Figure 3A) and the lack of a COPI interaction (no growth defects in *sey1*Δ *sec27-1*, *sey1*Δ *ret2-1*, and *sey1*Δ *cop1-1* mutants; Figure 3B and Supplemental Figure S1A). We also tested the third and final subunit of the Dsl1 complex, Tip20p, which was missing from the SGA analysis; *sey1*Δ *tip20-5* mutants exhibited strong synthetic growth defects, implicating the entire Dsl1 complex in ER–ER fusion (Figure 3C).

To test whether Dsl1p, Sec39p, and Tip20p function as a complex during ER–ER fusion, as they do during vesicle trafficking, we tested two additional *sey1*Δ *dsl1* mutants: *sey1*Δ *dsl1*-A533D and *sey1*Δ *dsl1*-L55E/L58D. In vitro, Dsl1p-A533D has a weakened interaction with Sec39p and Dsl1p-L55E/L58D has a weakened interaction with Tip20p (Ren *et al.*, 2009; Tripathi *et al.*, 2009). The *sey1*Δ *dsl1*-A533D double mutants exhibited a synthetic growth defect (Figure 3D), suggesting that the Dsl1-Sec39 interaction is required for SNARE-mediated ER–ER fusion. On the other hand, *sey1*Δ *dsl1*-L55E/L58D did not exhibit a synthetic growth defect (Figure 3D). This result is consistent with the ability of the same allele to support retrograde vesicle trafficking, as judged by its wild-type growth rate, and suggests that the *dsl1*-L55E/L58D mutation is not effective in disrupting the Dsl1 complex in vivo. Overall we conclude that the Dsl1 complex needs to be at least partially intact in order to participate in SNARE-mediated ER–ER fusion.

The Dsl1 complex is directly required for ER–ER fusion

It remained possible that the synthetic growth defects observed in *sey1*Δ *dsl1*ΔE double mutants were due to disruption of some other process required for normal growth, other than ER–ER fusion or vesicle trafficking. We therefore examined these mutants for ER structure defects that should arise from disrupted homotypic ER fusion. In wild-type cells, Sec63-GFP marks the entire ER network, which includes the nucleus, tubules extending from the nucleus to the cell cortex, and the tubules and sheets at the cell periphery. Sec63–green fluorescent protein (GFP) distribution appeared similar to wild type in *sey1*Δ and *dsl1*ΔE single mutants, but *sey1*Δ *dsl1*ΔE double mutants exhibited severely disrupted peripheral ER, lacking an organized tubular network and mostly appearing as patches or aggregates of peripheral ER (Figure 4A). The pool of ER near the plasma membrane is consistent with an inability for growing ER tubules to fuse at other parts of the ER network. Additionally, whereas in wild-type cells the ER forms an almost continuous network close

Allele	*sey1*Δ	*dsl1*ΔE	Description
*scs3*Δ	–0.84	–0.05	Protein required for inositol prototrophy
use1-TS	–0.65	–0.80	ER-localized SNARE required for retrograde vesicular traffic
sec39-1	–0.58	–0.91	Component of the Dsl1 tethering complex
sly1-TS	–0.54	–0.50	SM-family protein involved in ER/Golgi traffic
*pom33*Δ	–0.37	0.00	Transmembrane nucleoporin
sec23-1	–0.36	–0.05	COPII coat subunit, also stimulates the GTPase activity of Sar1p
*yop1*Δ	–0.32	–0.05	Membrane protein that interacts with Sey1p to maintain ER morphology
*ice2*Δ	–0.31	–0.29	Integral ER membrane protein with type-III transmembrane domains

Sorted list of *sey1*Δ-negative SGA scores, cutoff at –0.25.

TABLE 2: SGA scores of *sey1*Δ-negative genetic interactions.

to the plasma membrane, in *sey1*Δ *dsl1*ΔE mutant cells, we frequently observed large sections of the cortex with no ER and regions of ER internal to the cell.

We also assessed ER structure using Rtn1-GFP, which in wild-type cells localizes specifically to the tubular ER and the edges of sheets at the cell periphery and is excluded from the nucleus. Again, *sey1*Δ and *dsl1*ΔE single mutants appeared similar to wild type (Figure 4B). *sey1*Δ *dsl1*ΔE double mutants, however, exhibited a striking defect in which Rtn1-GFP accumulated in a few large, bright puncta, often at or near the bud neck (Figure 4B). As a measure of accumulation, the maximum fluorescence intensity of Rtn1-GFP in *sey1*Δ *dsl1*ΔE cells was ~10-fold higher than wild type (Figure 4B, top right), despite having only twofold higher total GFP (Figure 4B, bottom right). We occasionally observed a few long, unbranched ER tubules at the cell periphery (Figure 4B, *sey1*Δ *dsl1*ΔE peripheral enlargement), but the bright Rtn1-GFP aggregates near the bud neck usually obscured fluorescence signal at the periphery in most cells. Importantly, similar ER network defects were observed in *sey1*Δ *tip20-5* mutants but not *sey1*Δ *cop1-1* mutants (Figure S1B). Finally, we examined *sey1*Δ *dsl1*ΔE cells by electron microscopy and, consistent with our findings by fluorescence microscopy, observed abnormal ER in 53% of cells (random single sections through cells, $n = 38$; Figure S2A) and dense aggregates of ER-like membranes in 21% of cells (Figures 4C and S2B). Together these data demonstrate a perfect correlation between synthetic growth defects and synthetic ER structure defects, consistent with a causal relationship.

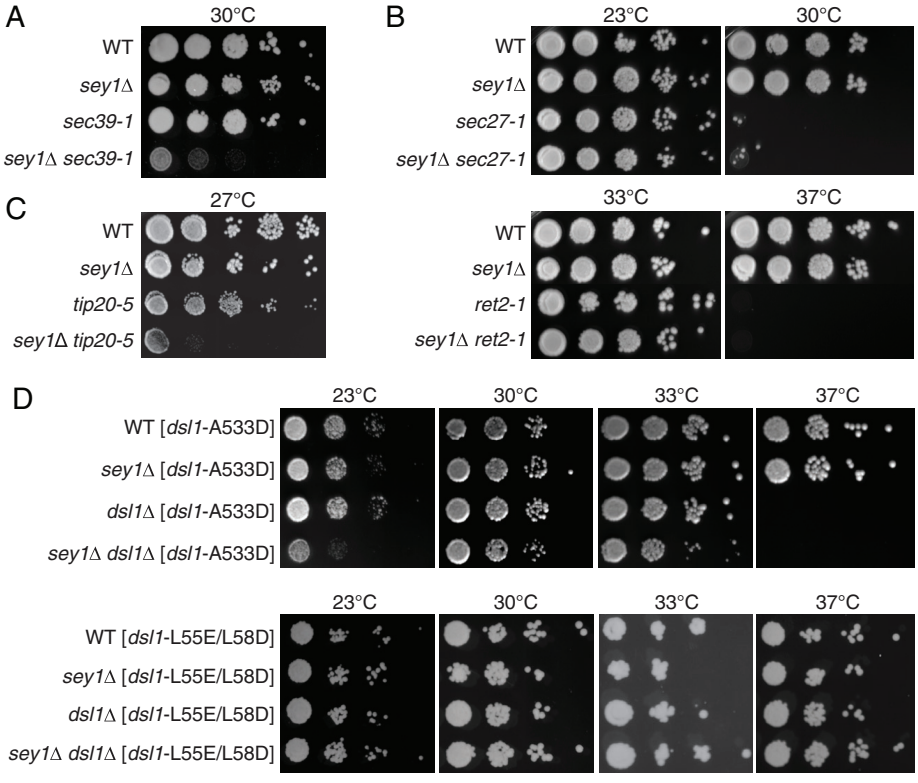

FIGURE 3: SNARE-mediated homotypic ER fusion requires the entire Dsl1 complex but not the COPI coat. (A) Growth assays of wild type (MY14289), *sey1*Δ (MY14291), *sec39-1* (MY14293), and *sey1*Δ *sec39-1* (MY14296) grown for 2 d at 30°C. (B) Top, wild type (MY14653), *sey1*Δ (MY14655), *sec27-1* (MY14657), and *sey1*Δ *sec27-1* (MY14659) grown for 3 d at 23°C and 2 d at 30°C. Bottom, wild type (MY14653), *sey1*Δ (MY14655), *ret2-1* (MY14661), and *sey1*Δ *ret2-1* (MY14663) grown at the indicated temperatures for 2 d. (C) Indicated genotypes derived from parent MY15008 grown for 2 d at 27°C. (D) Indicated genotypes with plasmid pRY270 (*dsl1*-A533D) or pRY261 (*dsl1*-L55E/L58D). Top, wild type (MY14365), *sey1*Δ (MY14369), *dsl1*Δ (MY14373), and *sey1*Δ *dsl1*Δ (MY14377). Bottom, wild type (MY14384), *sey1*Δ (MY14388), *dsl1*Δ (MY14392), and *sey1*Δ *dsl1*Δ (MY14396).

To address whether the Dsl1 complex directly mediates ER–ER fusion, rather than another step that modifies ER structure, we used a direct in vivo ER–ER fusion assay adapted from Anwar *et al.* (2012). In this assay, we mated cells containing cytosolic GFP and cells containing ER–lumenal mCherry (directed by a signal sequence and C-terminal ER-retention sequence, HDEL). For each mating pair, we collected images at 1-min intervals and determined the duration of the delay between cell fusion (marked by cytosolic GFP transfer) and ER–ER fusion (marked by mCherry transfer; Figure 5A). As previously demonstrated (Anwar *et al.*, 2012), ER–ER fusion required significantly more time in *sey1*Δ cells than in wild type (mean delay 8.7 vs. 4.9 min, $p = 0.01$, two-sample t test; Figure 5B). *dsl1*ΔE cells were not significantly different from wild type (5.3 vs. 4.9 min, $p = 0.81$). In contrast, ER–ER fusion

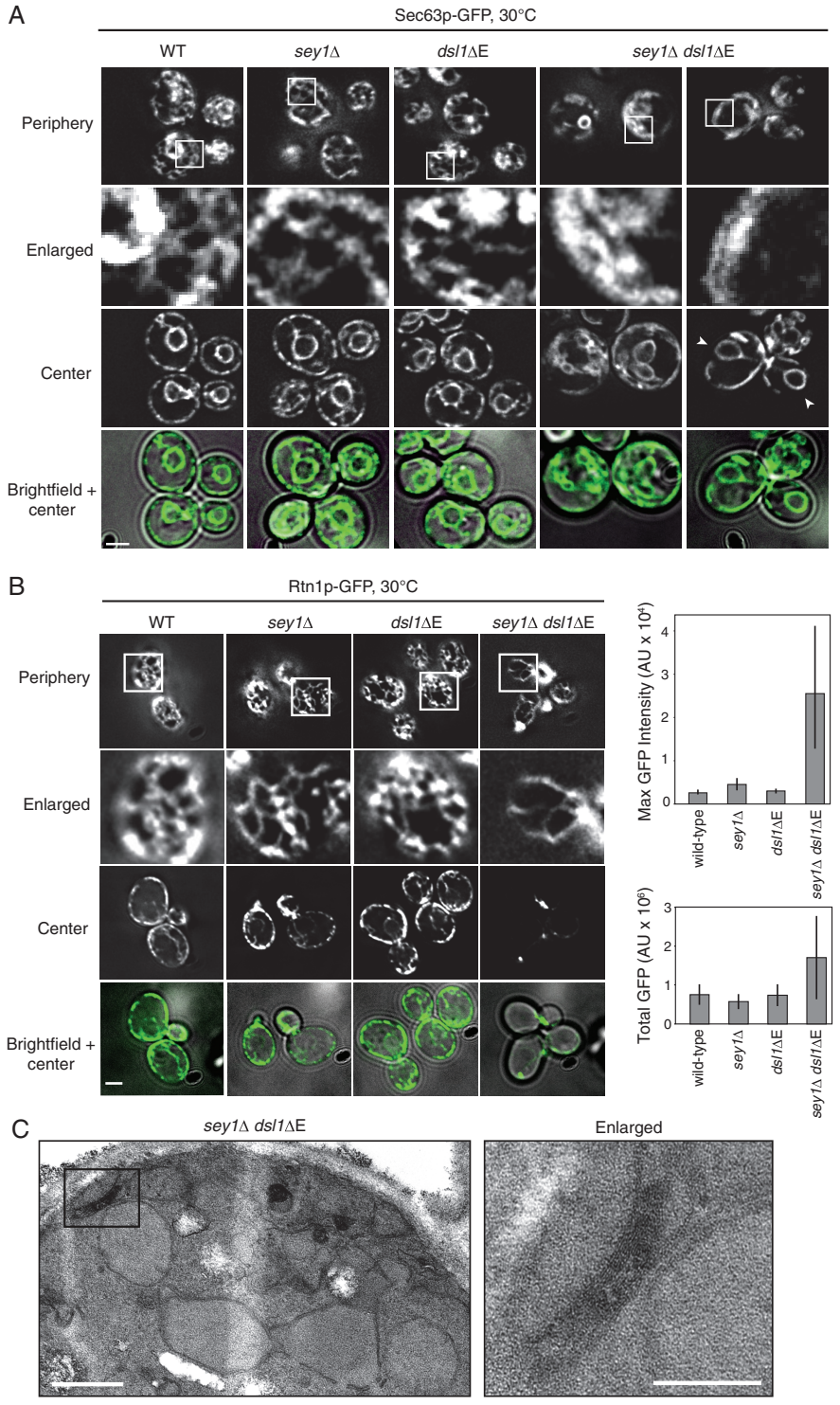

FIGURE 4: *sey1*Δ *dsl1*ΔE double mutants exhibit severe ER structure defects. (A) Cells expressing integrated Sec63p-GFP were grown to mid– to late log phase at 30°C in YEPD and imaged live (see *Materials and Methods* for image acquisition and analysis). Arrowheads depict large stretches of the cell periphery lacking ER. Haploid strains of the indicated genotype were derived from diploid parent MY14907. Enlarged panel images were sharpened in ImageJ (unsharp mask, 2.0 pixels, weight = 0.60). Scale bar: 2 µm. (B) Images as in A, but cells are expressing integrated Rtn1-GFP. Strains were derived from diploid parent MY15008. Scale bar: 2 µm. Top right graph: average (arbitrary units) and SD (error bars) of the maximum pixel intensity of each cell for the indicated genotype. Mean value and number of cells measured: WT, 2763 (22 cells); *sey1*Δ, 4586 (32 cells); *dsl1*ΔE, 3000 (37 cells); and *sey1*Δ *dsl1*ΔE, 26,439 (50 cells). *p* values vs. WT (two-sided Kolmogorov-Smirnov test): *sey1*Δ, 5×10^{-6}; *dsl1*ΔE, 0.28, *sey1*Δ *dsl1*ΔE, 4×10^{-13}. Bottom right graph: as above, but the sum of all pixel intensities was measured (including all *z*-slices). Mean value and *p* value vs. WT: WT, 0.75×10^6; *sey1*Δ, 0.57×10^6, $p = 0.03$; *dsl1*ΔE, 0.74×10^6, $p = 0.62$; and *sey1*Δ *dsl1*ΔE, 1.7×10^6, $p = 3 \times 10^{-6}$. All quantifications were performed in background-subtracted, raw images (not deconvolved). (C) Representative electron micrograph of ultrathin-sectioned *sey1*Δ *dsl1*ΔE cells (parent diploid MY14907), imaged at 10,000×. Scale bar: 500 nm. Right, 22,500× image of the region outlined in the black box in the left panel. Scale bar: 200 nm.

in *sey1*Δ *dsl1*ΔE mating pairs occurred ~24 min after wild type, an approximately fivefold increase ($p < 0.001$; Figure 5B). Because of the low-throughput nature of time-lapse microscopy, we performed a second assay in which we fixed the mating mixtures in paraformaldehyde and imaged the ER–lumenal mCherry distribution in many unbudded zygotes ($n > 50$ for each genotype for each experiment). While this assay is less sensitive to minor delays in ER–ER fusion, it allows a higher number of zygotes to be scored. We found that wild type, *sey1*Δ, and *dsl1*ΔE all appeared similar (<2% zygotes with unfused ER), whereas, in agreement with the results of the live-cell assay, *sey1*Δ *dsl1*ΔE zygotes displayed a dramatic deficiency in ER–ER fusion (62 ± 4% contained unfused ER; Figure 5C). Of note, ER–ER fusion was largely restored when *sey1*Δ *dsl1*ΔE cells were mated against wild type (Figure 5C). This initially seemed surprising, as ER–ER fusion presumably requires fusogens in both membranes; however, Dsl1p is soluble in the cytoplasm and likely equilibrates quickly between ER membranes. Together the ER structural defects and decreased ER–ER fusion rate demonstrate that the Dsl1 complex, in conjunction with the SNAREs and in parallel to Sey1p, plays a direct role in ER–ER fusion.

The reticulons are required for viability in a *sey1*Δ *dsl1*Δ*E* background

The reticulons Rtn1p, Rtn2p, and Yop1p are required for normal peripheral ER structure in vivo and can mediate ER tubule formation in vitro (Voeltz *et al.*, 2006; Hu *et al.*, 2008). Previous studies focusing only on Sey1p-mediated ER–ER fusion were unable to explain why *sey1*Δ *rtn1*Δ *rtn2*Δ *yop1*Δ mutants have only minor growth defects, despite having extremely perturbed ER structure (Voeltz *et al.*, 2006; West *et al.*, 2011). It was posited that either ER–ER fusion is not essential for viability under normal growth conditions in yeast or that there

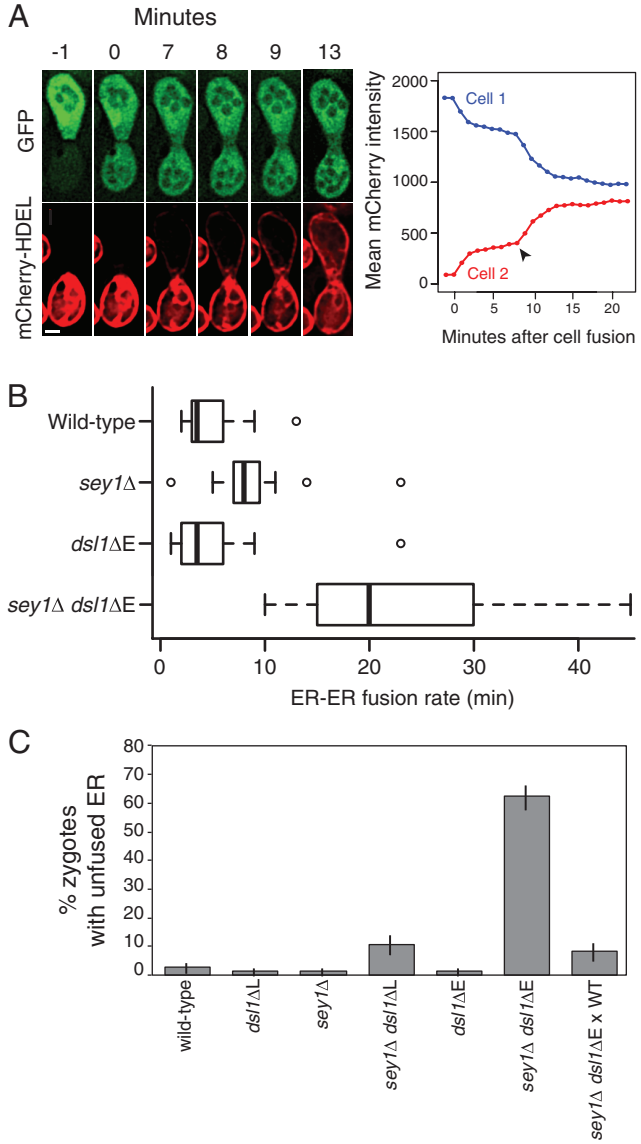

FIGURE 5: ER–ER fusion is severely delayed in *sey1*Δ *dsl1*ΔE mutants. (A) Representative example of the ER–ER fusion assay. Identical genotypes were mated to each other at room temperature; MATa strains expressed mCherry-HDEL (pMR6474), MATα strains expressed cytosolic GFP (pMR3619). *sey1*Δ cells are shown. The first peak in mCherry transfer at 0–2 min corresponds to the transfer of cytosolic mCherry-HDEL after cell fusion. Arrowhead depicts the point of ER–ER fusion (8 min). Scale bar: 2 μm. (B) Box plot of the times required for ER–ER fusion after cell fusion. Data are pooled from at least two independent experiments for each genotype. Mean values: wild type, 4.9 min (MY14509 × MY14513, $n = 16$); *sey1*Δ, 8.8 min (MY14510 × MY14514, $n = 16$); *dsl1*ΔE, 5.3 min (MY14511 × MY14515, $n = 14$); and *sey1*Δ *dsl1*ΔE, 23.4 min (MY14512 × MY14516; $n = 10$). Each box shows the interquartile range (25–75% of the data), black bars represent the median, and outliers are shown as open circles beyond the 1.5 * interquartile range. (C) Percentage of zygotes with unfused ER (binary scoring). The data are pooled from two independent experiments; error bars show ± SE for a binomial distribution. Strains used: wild type (MY14059 × MY14009), *dsl1*ΔL (MY14061 × MY14013), *sey1*Δ (MY14063 × MY14017), *sey1*Δ *dsl1*ΔL (MY14065 × MY14021), *dsl1*ΔE (MY14067 × MY14025), *sey1*Δ *dsl1*ΔE (MY14071 × MY14031), and *sey1*Δ *dsl1*ΔE (MY14071) × wild type (MY14009). All MATa strains expressed GFP-HDEL (pMR6473).

exists an alternative ER–ER fusion pathway. Despite the identification of an alternative SNARE/Dsl1-mediated ER–ER fusion pathway, *sey1*Δ *dsl1*ΔE double mutants, which have lost two ER–ER fusion pathways, remain viable (albeit slow growing). It therefore remained possible that ER–ER fusion is a nonessential process in yeast.

To address this possibility and to explore the relationship, if any, between the reticulons and the SNARE/Dsl1-mediated ER–ER fusion pathway, we dissected ~100 tetrads from a diploid heterozygous for *sey1*Δ, *rtn1*Δ, *rtn2*Δ, *yop1*Δ, *lnp1*Δ, and *dsl1*ΔE, and quantified colony growth over time of the different genetic combinations, averaged by genotype. We observed a minimal effect of *rtn2*Δ on the growth rate relative to any comparable genetic combination (Figure S3, A and B; see Table S2 for full growth data), consistent with Rtn2p's low level of expression under normal growth conditions (De Craene *et al.*, 2006; Voeltz *et al.*, 2006). We therefore averaged colony sizes independently of *RTN2*. Additionally, our results recapitulated published growth defects of *lnp1*Δ *rtn1*Δ and suppression of *lnp1*Δ *rtn1*Δ by *sey1*Δ (Figure S3C; Chen *et al.*, 2012). *lnp1*Δ was included in our analysis, as Lnp1p was previously shown to antagonize Sey1p activity via an unknown mechanism (Chen *et al.*, 2012). However, there were no synthetic genetic interactions between *lnp1*Δ and *dsl1*ΔE, and we therefore do not discuss *LNP1* further (Figure S3C).

We next compared growth rates related only to *sey1*Δ, *rtn1*Δ, *yop1*Δ, and *dsl1*ΔE genotypic combinations (Figure 6A). As expected, all single mutants grew about as well as wild type (compare strain 1 with strains 2–5 in Figure 6A). Among double mutants (strains 6–11), *sey1*Δ *dsl1*ΔE exhibited a strong growth defect, as expected from our initial work, and *yop1*Δ *rtn1*Δ exhibited a minor growth defect, as previously reported. Surprisingly, *rtn1*Δ *dsl1*ΔE exhibited an intermediate growth defect, implying that Rtn1p and Dsl1p share functional redundancy. All triple mutants (strains 12–15) showed intermediate to severe growth defects (see Figure 6B for colony sizes after 6 d of growth). The quadruple-mutant *sey1*Δ *yop1*Δ *rtn1*Δ *dsl1*ΔE (strain 16) was almost completely inviable (four out of eight spores did not form colonies after 6 d of growth, and the remaining spores formed extremely tiny colonies; Figure 6B), suggesting that there is an unexpected partial redundancy between the function of the reticulons and the two ER–ER fusion pathways, which together are essential for cell viability.

It is thought that the reticulons both generate and maintain ER tubules and thus may act genetically in the same pathway with Sey1p (Hu *et al.*, 2009; Chen *et al.*, 2012). The relationship between SNARE-mediated ER–ER fusion and the reticulons, however, is unclear. Because the *sey1*Δ *yop1*Δ *rtn1*Δ *dsl1*ΔE quadruple mutant (strain 16) is almost inviable, The Dsl1 pathway must be responsible for the relatively normal growth rate of the *sey1*Δ *yop1*Δ *rtn1*Δ triple mutant (strain 12). We conclude, therefore, that SNARE/Dsl1-mediated ER–ER fusion does not require the reticulons Rtn1p and Yop1p (Figure 6A). Conversely, Sey1p is less able than Dsl1p to support reticulon-independent growth, as cells that are only *SEY1*+ (*yop1*Δ *rtn1*Δ *dsl1*ΔE, strain 15) have a more severe growth defect than cells that are only *DSL1*+ (*sey1*Δ *yop1*Δ *rtn1*Δ, strain 12). Notably, however, *SEY1* still confers a growth advantage on cells lacking reticulons and wild-type DSL1 (Figure 6B, compare strains 15 and 16). Finally, when *dsl1*ΔE is combined with *sey1*Δ, *rtn1*Δ, or both *sey1*Δ and *rtn1*Δ, the resulting growth defects are all similar (Figure 6A, compare strains 8, 11, and 14), suggesting that Sey1p and Rtn1p share a genetic pathway distinct from Dsl1p.

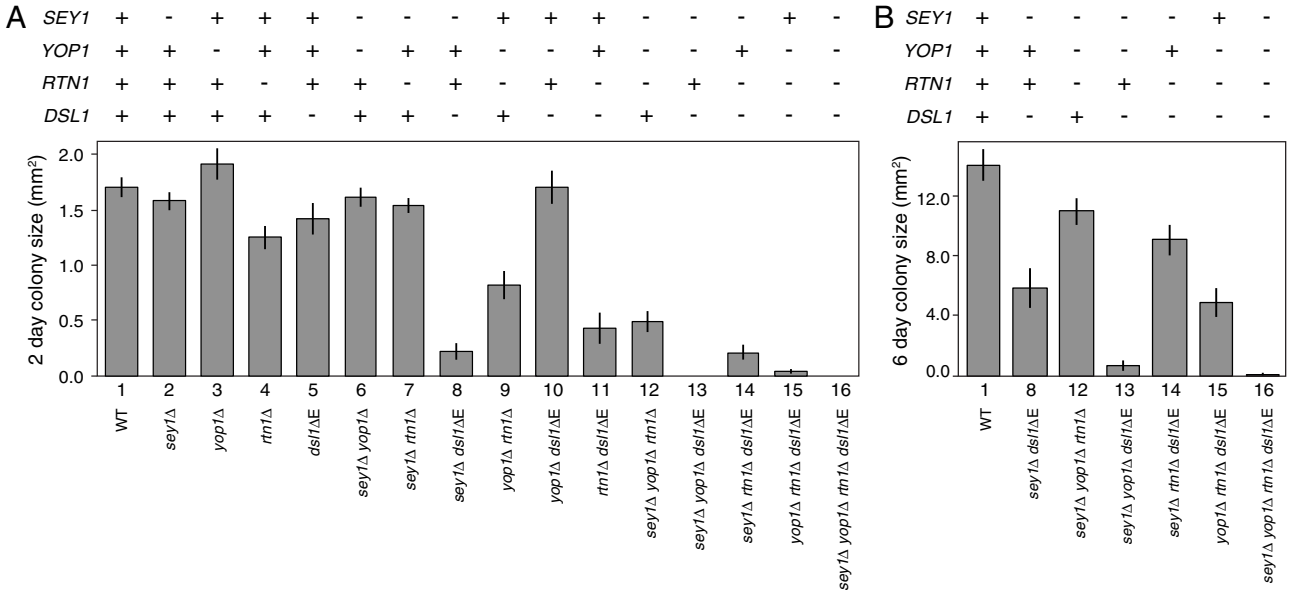

FIGURE 6: The reticulons are required for viability in a *sey1*Δ *dsl1*ΔE background. (A) Colony sizes after tetrad dissection (parent MY14454) and 48 h of growth at 30°C on YEPD for the indicated genotypes. All genotypes are *LNP1+* and averaged independently of *RTN2*. Number of colonies averaged for each genotype ranged from 6 to 18 (see Table S2 for full data). Errors bars show ± SE of the mean. (B) As in A, but after 6 d of growth at 30°C.

A surprising observation was that cells that are only *YOP1+* (*sey1*Δ *rtn1*Δ *dsl1*ΔE, strain 14) have an intermediate growth defect, whereas cells that are only *RTN1+* (*sey1*Δ *yop1*Δ *dsl1*ΔE, strain 13) are almost inviable (Figure 6B). Therefore Yop1p but not Rtn1p can contribute substantially to cell growth independently of the other reticulons and of the Sey1p- and SNARE/Dsl1-dependent ER–ER fusion pathways.

DISCUSSION

Characterization of SNARE-mediated homotypic ER fusion

On the basis of synthetic growth defects and ER–ER fusion experiments in this study, we conclude that SNARE-mediated homotypic ER fusion additionally requires the Dsl1 complex, consisting of Sec39p, Dsl1p, and Tip20p. Furthermore, genetic analysis indicates that the observed synthetic defects are not indirectly caused by perturbed vesicle trafficking; if they were, then other mutations that disrupt vesicle trafficking, such as mutations in vesicle coat components or other SNAREs, should have resulted in growth and ER structure defects in a *sey1*Δ background (see Table S1 for full list of trafficking components tested). These results imply that SNARE-mediated ER–ER fusion occurs independently of vesicle fusion and relies on direct ER–ER interactions, similar to the model for Sey1p-mediated ER–ER fusion (Figure 7).

In the Dsl1 complex mutants examined in this study, there was a perfect correlation between synthetic growth defects and synthetic ER structure and ER–ER fusion defects. It is conceivable that aberrant ER structures could inhibit the observed rate of ER–ER fusion in our assay, but we note that previous reports demonstrated that *rtn1*Δ *rtn2*Δ *yop1*Δ mutants, which have severe ER structure defects, have a normal rate of ER–ER fusion (Anwar *et al.*, 2012). Therefore we conclude that the SNAREs most likely act with the Dsl1 complex as true fusogens for homotypic ER fusion.

The full composition of the ER–ER fusion SNARE complex is not yet clear. Only three SNARE genes—*SEC20*, *USE1*, and *UFE1*—have shown genetic interactions with *SEY1*, whereas a normal four-helix SNARE complex requires four SNARE proteins. In retrograde trafficking, Sec22p is the fourth SNARE, but Ykt6p can compensate in cells lacking Sec22p (Liu and Barlowe, 2002). Sec22p/Ykt6p could also redundantly mediate ER–ER fusion, but this is difficult to test, as known *sec22 ykt6* double mutants are either inviable or severely slow growing (Liu and Barlowe, 2002; Rogers *et al.*, 2013).

During retrograde trafficking, the Dsl1 complex tethers ER-bound SNAREs to the incoming COPI-coated vesicle and promotes *trans*-SNARE complex assembly. Our results imply that the Dsl1 complex uses a coat-independent function during ER–ER fusion. In agreement with this conclusion, *dsl1-4* mutants accumulate ER and vesicles at the nonpermissive temperature, whereas *dsl1-7* mutants accumulate only ER, suggesting that Dsl1p has two different functions (VanRheenen *et al.*, 2001). Furthermore, overexpression of Sec21p (γ-COP), a COPI complex subunit, suppressed the lethality of *dsl1-4* but not *dsl1-7*, supporting a COPI-independent role for Dsl1p (VanRheenen *et al.*, 2001). Mechanistically, because the Dsl1 complex promotes SNARE complex formation and stabilization, this mechanism could apply to ER–ER fusion as well, independent of a vesicle-tethering function (Ren *et al.*, 2009; Diefenbacher *et al.*, 2011). An attractive hypothesis is that the Dsl1p complex might adopt an extended conformation that tethers SNAREs residing on the two apposing ER membranes before fusion.

The SNARE/Dsl1-mediated homotypic ER fusion pathway characterized here may have additional components that are not shared with retrograde vesicle trafficking. Such components should exhibit negative genetic interactions with *sey1*Δ. Only five candidates were identified (Table 2): *yop1*Δ, *ice2*Δ, *scs3*Δ, *pom33*Δ, and *sec23*-1. Yop1p and Ice2p broadly affect ER structure and function and may not be specific to SNARE-mediated ER–ER fusion. Scs3p is required for normal ER membrane biosynthesis and exhibits genetic interactions with many cellular processes, suggesting that it too may not be specific for SNARE-mediated ER–ER fusion (Hosaka *et al.*, 1994; Moir *et al.*, 2012). Pom33p is a transmembrane nucleoporin (Chadrin *et al.*, 2010). Interestingly, some reticulons have additional roles in nuclear pore complex biogenesis in addition to ER tubulation, probably via a common curvature-inducing mechanism (Dawson *et al.*, 2009). Furthermore, Rtn1p and Yop1p physically

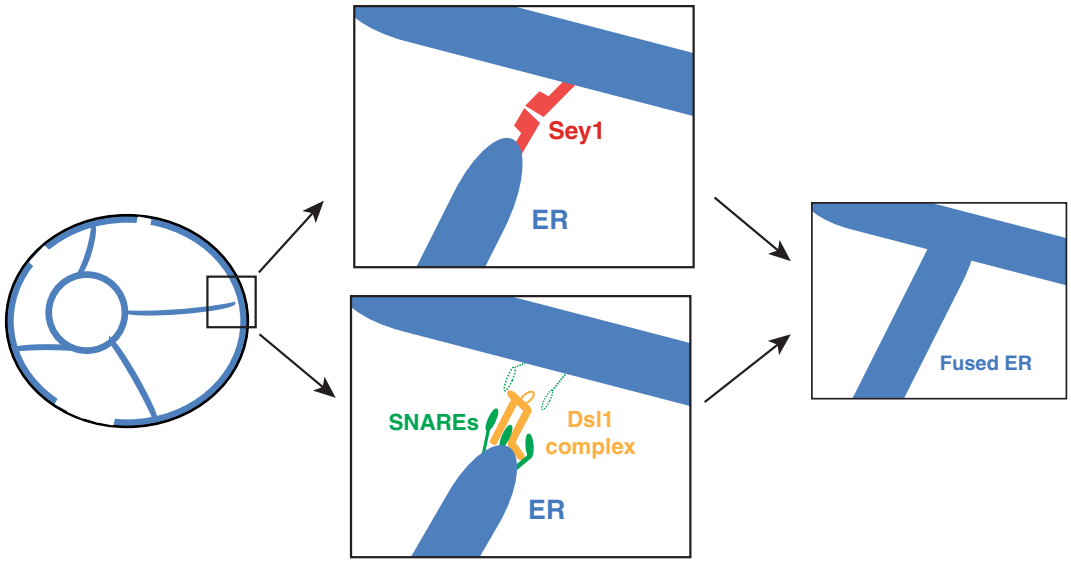

FIGURE 7: Model for homotypic ER fusion. The left-most panel depicts the ER network (blue) within a typical yeast cell (black outline). A few tubules connect the nuclear ER to the peripheral ER, which is discontinuous when viewed as a slice. The two middle panels depict alternative homotypic ER fusion pathways for an ER tubule. Either pathway leads to the same outcome, depicted in the right-most panel: the creation of a new three-way junction. The top middle panel depicts canonical Sey1p-mediated ER–ER fusion. The bottom middle panel depicts SNARE/Dsl1 complex–mediated homotypic ER fusion, as defined in this study. The two dotted-line SNAREs represent uncertainty in the exact composition and topology of the final SNARE complex.

interact with Ndc1p, a component of nuclear pore complexes (Casey *et al.*, 2012). Therefore *sey1*Δ *pom33*Δ double mutants may have disrupted nuclear pore complex functions. However, as SNARE-mediated ER–ER fusion must occur at the peripheral ER, away from the nucleus, a role for Pom33p at the peripheral ER would be surprising. Finally, Sec23p is a component of the COPII coat that stimulates the GTPase activity of Sar1p and is required for ER-to-Golgi anterograde vesicle trafficking. However, all other anterograde trafficking components, including the rest of the COPII coat, do not genetically interact with *sey1*Δ (except *sar1*, for which we have no data; Table S1). It is therefore possible that Sec23p has a novel, vesicle-independent function in SNARE-mediated ER–ER fusion.

Finally, we note that all identified members of SNARE-mediated ER–ER fusion have conserved mammalian orthologues, raising the possibility that this pathway is conserved among eukaryotes (conservation reviewed in Schmitt, 2010).

Functional overlap between Sey1p-mediated and SNARE-mediated ER–ER fusion

An open question is whether Sey1p and SNAREs mediate distinct ER–ER fusion events. *sey1*Δ and *dsl1*ΔE single mutants exhibit no growth defects, and *sey1*Δ mutants have only minor defects in ER structure and ER–ER fusion rate compared with *sey1*Δ *dsl1*ΔE double mutants. This suggests that under normal growth conditions the two pathways are largely, but not entirely, redundant and independent. However, it is possible that one pathway is favored under certain environmental conditions, such as different osmolarities or temperatures, or that they mediate fusion at ER domains that have subtle differences.

The function of ER structure and fusion in yeast cells

An early mystery in our study was why *sey1*Δ *dsl1*ΔE double mutants are viable if both ER–ER fusogens have been disrupted. We reasoned that this could be because 1) the *dsl1*ΔE mutation only partially disrupts SNARE-mediated ER–ER fusion; 2) there is a third, redundant ER–ER fusion pathway; or 3) ER–ER fusion is not an essential process for yeast viability under normal growth conditions. The first possibility is difficult to test, as all of the genes in the SNARE/Dsl1 pathway are essential and cannot be deleted. The second possibility, that there is a third, albeit inefficient, fusogen, is supported by the observation that Yop1p is required for most of the remaining growth in the *sey1*Δ *dsl1*ΔE double mutant. Therefore Yop1p may be an essential member of a third ER–ER fusion pathway, or Yop1p itself may function as both a reticulon and a weak fusogen. The latter interpretation is supported by the finding that Yop1p is sufficient to form both tubules and three-way ER junctions in vitro, whereas Rtn1p only forms tubules and no junctions (Hu *et al.*, 2008). The third possibility, that ER–ER fusion is not an essential process under our growth conditions, remains formally plausible, as even *sey1*Δ *rtn1*Δ *yop1*Δ *dsl1*ΔE mutants occasionally formed tiny colonies after ~6 d of growth at 30°C (four out of eight spores). However, this conclusion assumes there is no fourth fusogen, that ER–ER fusion will not spontaneously occur without a fusogen, and that the *dsl1*ΔE mutation fully disrupts SNARE-mediated ER–ER fusion.

A remaining problem is identifying the most proximal cause of the *sey1*Δ *dsl1*ΔE growth defect. Disrupted ER–ER fusion could affect multiple downstream processes, including ER inheritance, lipid homeostasis between the nuclear and peripheral ER, and protein recycling. In such cases, one should be able to restore normal growth by rescuing the downstream processes without rescuing ER–ER fusion itself. More indirectly, accumulated ER could physically block exo/endocytosis at the plasma membrane, or organelle or nuclear segregation, as was observed for *sey1*Δ mutants during nuclear congression during mating (Rogers *et al.*, 2013). Discerning these mechanisms should prove fruitful in future studies.

MATERIALS AND METHODS

Strains and general yeast methods

Strains and plasmids used are listed in Table S3. Standard methods including cell culture and transformations were performed as

described by Amberg *et al.* (2005). In general, many of the slow-growing strains described in this study were prone to accumulating intermediate suppressors of growth rate if used for many generations. To avoid this confounding issue, we sometimes generated desired genotypes for an experiment from a heterozygous diploid parent as stated in the figure legends but did not freeze the haploids as separate strains.

Growth assays

Cultures were grown to saturation in yeast extract/peptone/dextrose (YEPD) at 23°C (except 30°C for the assay in Figure 1B) and then 0.2 OD_{600} unit of cells was pelleted and resuspended in 200 µl dH_2O. Five 10-fold serial dilutions were made in a 96-well plate and then spotted on YEPD plates and grown at various temperatures as indicated.

SGA experiments and analysis

*dsl1*ΔE:NatMX (MY15059), *dsl1*ΔLasso:NatMX (MY15060), and *DSL1*+::NatMX (MY15058) strains were created using parent strain Y7092, and SGA screens were performed and analyzed as previously described (Tong and Boone, 2006; Baryshnikova *et al.*, 2010). SGA screens with temperature-sensitive alleles were performed at 26°C. To separate the alleles into classes, we used a cutoff score (requiring at least one SGA score with an absolute value ≥ 0.25) and a difference threshold (requiring that SGA scores differed by at least an absolute value of 0.25 to be classified as specific). Additionally, for the alleles in the shared class, we required that both SGA scores had an absolute value of at least 0.25.

Image acquisition and analysis

All microscopy was performed on a DeltaVision deconvolution microscope (Applied Precision, Issaquah, WA), based on a Nikon TE200 (Melville, NY) with an inverted 100× NA 1.4 objective, a 50-W mercury lamp, and a Photometrics Cool Snap HQ CCD camera (Photometrics, Tucson, AZ). All images were deconvolved using the Applied Precision SoftWoRx imaging software.

ER structure microscopy

Cells were imaged live in growth medium at room temperature on a standard glass slide and #1.5 coverslip. Typically, imaging began at the bottom of a cell (nearest the objective and touching the coverslip) and 30–40 slices were imaged with 0.15-µm *z*-spacing. Exposure times were typically 0.5–1.0 s, except *sey1*Δ *dsl1*ΔE and *sey1*Δ *tip20-5* cells expressing Rtn1-GFP (Figures 4B and S1B) were imaged at 0.05–0.1 s to avoid pixel saturation.

ER–ER fusion assays

Cultures were grown overnight to early to mid–log phase in synthetic complete medium lacking leucine (SC –leu) at 30°C. Cells from each strain to be mated (0.01 OD_{600} unit) were added onto a pretreated 0.17-mm Delta T4 Culture Dish (Bioptechs, Butler, PA). Immediately before the cells were added, the Delta-T dishes were pretreated by coating with 25 µl of concanavalin A (0.1 mg/ml in 20 mM sodium acetate, pH 5.8) for 15 min and then being washed twice with 50 µl of 20 mM sodium acetate (pH 5.8). Cells were allowed to settle for 15 min before being washed with 200 µl of SC –leu to remove unstuck cells. Finally, 2 ml of SC –leu was added to the dish, and matings were imaged at room temperature. Mating pairs were imaged at 1-min intervals with minimal exposure times (usually 0.1 s) and at a single focal plane to reduce photobleaching and phototoxicity. After imaging, raw movies (not deconvolved) were scored for the time between cell fusion and ER–ER fusion. Cell fusion was identified by a rapid transfer of cytoplasmic GFP into the adjacent mating partner that usually equilibrated in less than 2 min. The first time point with cytoplasmic GFP in both cells, even if not yet equilibrated, was marked as the time of cell fusion. After cell fusion, mCherry-HDEL accumulated slowly in the mating partner's cytoplasm and ER, presumably due to cytoplasmic mCherry-HDEL and protein recycling. Eventually mCherry-HDEL transfer shifted to a rapid equilibration phase (see Figure 5A and Anwar *et al.*, 2012). The first time point with this shift to fast equilibration was marked as the time of ER–ER fusion.

Fixed-cell assays (Figure 5C) were performed as previously described (Rogers *et al.*, 2013). Briefly, cultures were grown at 30°C to mid–log phase, and 0.5 OD_{600} unit of cells was mixed and mated on a 0.45-µm nitrocellulose filter (EMD Millipore, Billerica, MA) for 3 h at 23°C. Cells were then washed into 900 µl of 1× phosphate-buffered saline (PBS), and 100 µl of 20% paraformaldehyde dissolved in distilled H_2O was added. Cells were fixed at room temperature for 15 min; this was followed by one wash in 1× PBS, 4′,6-diamidino-2-phenylindole staining (2 µg/ml in PBS) for 15 min, two more washes in 1× PBS, and, finally, resuspension in 100–200 µl 1× PBS. Cells were imaged on the same day. GFP-HDEL was used in the fixed-cell assay rather than mCherry-HDEL, as GFP-HDEL intensity and localization is preserved better after fixation. Imaging on the same day ensures that the membranes stay intact and GFP-HDEL does not artifactually diffuse to equilibrium. ER was scored as unfused when GFP-HDEL appeared markedly brighter in one-half of the zygote than the other.

Electron microscopy

Cells were prepared for transmission electron microscopy as described in Gammie and Rose (2002). Briefly, the workflow included a glutaraldehyde fixation, potassium permanganate staining, sodium periodate treatment, uranyl acetate staining, and embedding in LR White resin. Specifically to our protocol, ~5 OD_{600} units of mid–log phase *sey1*Δ *dsl1*ΔE cells (from diploid parent MY14907) were fixed in 2% glutaraldehyde for 30 min at room temperature. Cells were stained with 4% potassium permanganate for 4 h at 4°C. Ultrathin sections (~80 nm) were placed on a nickel slotted-grid (Formvar film, FF-2010-Ni, Electron Microscopy Sciences, Hatfield, PA) and imaged directly, without lead citrate staining.

Colony size time-course analysis

Strain MY14454 was sporulated, and 100 tetrads were dissected on YEPD plates. The plates were incubated at 30°C and imaged after 2, 3, 4, 5, and 6 d of growth. Colony size was measured in ImageJ by applying a binary threshold mask to outline colonies. After 6 d, plates were replica plated to determine genotypes. Genotypes for lethal or extremely tiny colonies were inferred by assuming 2:2 segregation of genes. We excluded from our analysis tetrads that did not exhibit 2:2 segregation for all genes or tetrads that did not permit unambiguous determination of all four spores (e.g., only two cells were viable in the tetrad).

ACKNOWLEDGMENTS

We thank members of the Rose, Gammie, Hughson, and Boone laboratories for helpful support and discussion. We also thank S. Ferro-Novick for providing parent strains used in this study and Bryan-Joseph San Luis for technical assistance. This work was supported by National Institutes of Health grants GM037739 (to M.D.R.) and GM071574 (to F.M.H.). J.V.R. was supported by National Institutes of Health training grant GM007388.

REFERENCES

Amberg D, Burke J, Strathern J (2005). Methods in Yeast Genetics, Cold Spring Harbor, NY: Cold Spring Harbor Laboratory Press.

Andag U, Neumann T, Schmitt HD (2001). The coatomer-interacting protein Dsl1p is required for Golgi-to-endoplasmic reticulum retrieval in yeast. J Biol Chem 276, 39150–39160.

Andag U, Schmitt HD (2003). Dsl1p, an essential component of the Golgi-endoplasmic reticulum retrieval system in yeast, uses the same sequence motif to interact with different subunits of the COPI vesicle coat. J Biol Chem 278, 51722–51734.

Anwar K, Klemm RW, Condon A, Severin KN, Zhang M, Ghirlando R, Hu J, Rapoport TA, Prinz WA (2012). The dynamin-like GTPase Sey1p mediates homotypic ER fusion in *S. cerevisiae*. J Cell Biol 197, 209–217.

Baryshnikova A, Costanzo M, Dixon S, Vizeacoumar FJ, Myers CL, Andrews B, Boone C (2010). Synthetic genetic array (SGA) analysis in *Saccharomyces cerevisiae* and *Schizosaccharomyces pombe*. Methods Enzymol 470, 145–179.

Burri L, Lithgow T (2004). A complete set of SNAREs in yeast. Traffic 5, 45–52.

Casey AK, Dawson TR, Chen J, Friederichs JM, Jaspersen SL, Wente SR (2012). Integrity and function of the *Saccharomyces cerevisiae* spindle pole body depends on connections between the membrane proteins Ndc1, Rtn1, and Yop1. Genetics 192, 441–455.

Chadrin A, Hess B, San Roman M, Gatti X, Lombard B, Loew D, Barral Y, Palancade B, Doye V (2010). Pom33, a novel transmembrane nucleoporin required for proper nuclear pore complex distribution. J Cell Biol 189, 795–811.

Chen S, Novick P, Ferro-Novick S (2012). ER network formation requires a balance of the dynamin-like GTPase Sey1p and the Lunapark family member Lnp1p. Nat Cell Biol 14, 707–716.

Chen S, Novick P, Ferro-Novick S (2013). ER structure and function. Curr Opin Cell Biol 25, 428–433.

Costanzo M, Baryshnikova A, Bellay J, Kim Y, Spear ED, Sevier CS, Ding H, Koh JL, Toufighi K, Mostafavi S, *et al.* (2010). The genetic landscape of a cell. Science 327, 425–431.

Dawson TR, Lazarus MD, Hetzer MW, Wente SR (2009). ER membrane-bending proteins are necessary for de novo nuclear pore formation. J Cell Biol 184, 659–675.

De Craene J-O, Coleman J, Estrada de Martin P, Pypaert M, Anderson S, Yates JR, Ferro-Novick S, Novick P (2006). Rtn1p is involved in structuring the cortical endoplasmic reticulum. Mol Biol Cell 17, 3009–3020.

Delic M, Valli M, Graf AB, Pfeffer M, Mattanovich D, Gasser B (2013). The secretory pathway: exploring yeast diversity. FEMS Microbiol Rev 37, 872–914.

Diefenbacher M, Thorsteinsdottir H, Spang A (2011). The Dsl1 tethering complex actively participates in soluble NSF (N-ethylmaleimide-sensitive factor) attachment protein receptor (SNARE) complex assembly at the endoplasmic reticulum in *Saccharomyces cerevisiae*. J Biol Chem 286, 25027–25038.

English AR, Voeltz GK (2013). Endoplasmic reticulum structure and interconnections with other organelles. Cold Spring Harb Perspect Biol 5, a013227.

Estrada de Martin P, Du Y, Novick P, Ferro-Novick S (2005). Ice2p is important for the distribution and structure of the cortical ER network in *Saccharomyces cerevisiae*. J Cell Sci 118, 65–77.

Gammie AE, Rose MD (2002). Assays of cell and nuclear fusion. Methods Enzymol 351, 477–498.

Hong W, Lev S (2014). Tethering the assembly of SNARE complexes. Trends Cell Biol 24, 35–43.

Hosaka K, Nikawa J, Kodaki T, Ishizu H, Yamashita S (1994). Cloning and sequence of the *SCS3* gene which is required for inositol prototrophy in *Saccharomyces cerevisiae*. J Biochem 116, 1317–1321.

Hu J, Shibata Y, Voss C, Shemesh T, Li Z, Coughlin M, Kozlov MM, Rapoport T A, Prinz W A (2008). Membrane proteins of the endoplasmic reticulum induce high-curvature tubules. Science 319, 1247–1250.

Hu J, Shibata Y, Zhu P-P, Voss C, Rismanchi N, Prinz WA, Rapoport TA, Blackstone C (2009). A class of dynamin-like GTPases involved in the generation of the tubular ER network. Cell 138, 549–561.

Jedd G, Richardson C, Litt R, Segev N (1995). The Ypt1 GTPase is essential for the first two steps of the yeast secretory pathway. J Cell Biol 131, 583–590.

Kamena F, Diefenbacher M, Kilchert C, Schwarz H, Spang A (2008). Ypt1p is essential for retrograde Golgi-ER transport and for Golgi maintenance in *S. cerevisiae*. J Cell Sci 121, 1293–1302.

Kraynack BA, Chan A, Rosenthal E, Essid M, Umansky B, Waters MG, Schmitt HD (2005). Dsl1p, Tip20p, and the novel Dsl3(Sec39) protein are required for the stability of the Q/t-SNARE complex at the endoplasmic reticulum in yeast. Mol Biol Cell 16, 3963–3977.

Lee C, Chen LB (1988). Dynamic behavior of endoplasmic reticulum in living cells. Cell 54, 37–46.

Li Y, Gallwitz D, Peng R (2005). Structure-based functional analysis reveals a role for the SM protein Sly1p in retrograde transport to the endoplasmic reticulum. Mol Biol Cell 16, 3951–3962.

Liu Y, Barlowe C (2002). Analysis of Sec22p in endoplasmic reticulum/Golgi transport reveals cellular redundancy in SNARE protein function. Mol Biol Cell 13, 3314–3324.

Moir RD, Gross DA, Silver DL, Willis IM (2012). SCS3 and YFT2 link transcription of phospholipid biosynthetic genes to ER stress and the UPR. PLoS Genet 8, e1002890.

Orso G, Pendin D, Liu S, Tosetto J, Moss TJ, Faust JE, Micaroni M, Egorova A, Martinuzzi A, McNew JA, Daga A (2009). Homotypic fusion of ER membranes requires the dynamin-like GTPase atlastin. Nature 460, 978–983.

Ossig R, Dascher C, Trepte HH, Schmitt HD, Gallwitz D (1991). The yeast SLY gene products, suppressors of defects in the essential GTP-binding Ypt1 protein, may act in endoplasmic reticulum-to-Golgi transport. Mol Cell Biol 11, 2980–2993.

Patel SK, Indig FE, Olivieri N, Levine ND, Latterich M (1998). Organelle membrane fusion: a novel function for the syntaxin homolog Ufe1p in ER membrane fusion. Cell 92, 611–620.

Ren Y, Yip CK, Tripathi A, Huie D, Jeffrey PD, Walz T, Hughson FM (2009). A structure-based mechanism for vesicle capture by the multisubunit tethering complex Dsl1. Cell 139, 1119–1129.

Rogers JV, Arlow T, Inkellis ER, Koo TS, Rose MD (2013). ER-associated SNAREs and Sey1p mediate nuclear fusion at two distinct steps during yeast mating. Mol Biol Cell 24, 3896–3908.

Sandrock TM, O'Dell JL, Adams AE (1997). Allele-specific suppression by formation of new protein-protein interactions in yeast. Genetics 147, 1635–1642.

Schmitt HD (2010). Dsl1p/Zw10: common mechanisms behind tethering vesicles and microtubules. Trends Cell Biol 20, 257–268.

Schuldiner M, Weissman JS (2013). The contribution of systematic approaches to characterizing the proteins and functions of the endoplasmic reticulum. Cold Spring Harb Perspect Biol 5, a013284.

Shibata Y, Voss C, Rist JM, Hu J, Rapoport TA, Prinz WA, Voeltz GK (2008). The reticulon and DP1/Yop1p proteins form immobile oligomers in the tubular endoplasmic reticulum. J Biol Chem 283, 18892–18904.

Spang A (2013). Retrograde traffic from the Golgi to the endoplasmic reticulum. Cold Spring Harb Perspect Biol 5, a013391.

Sutton RB, Fasshauer D, Jahn R, Brunger AT (1998). Crystal structure of a SNARE complex involved in synaptic exocytosis at 2.4 A resolution. Nature 395, 347–353.

Tong AHY, Boone C (2006). Synthetic genetic array analysis in *Saccharomyces cerevisiae*. Methods Mol Biol 313, 171–192.

Tripathi A, Ren Y, Jeffrey PD, Hughson FM (2009). Structural characterization of Tip20p and Dsl1p, subunits of the Dsl1p vesicle tethering complex. Nat Struct Mol Biol 16, 114–123.

VanRheenen SM, Reilly BA, Chamberlain SJ, Waters MG (2001). Dsl1p, an essential protein required for membrane traffic at the endoplasmic reticulum/Golgi interface in yeast. Traffic 2, 212–231.

Voeltz GK, Prinz WA, Shibata Y, Rist JM, Rapoport T A (2006). A class of membrane proteins shaping the tubular endoplasmic reticulum. Cell 124, 573–586.

Weber T, Zemelman B V, McNew JA, Westermann B, Gmachl M, Parlati F, Söllner TH, Rothman JE (1998). SNAREpins: minimal machinery for membrane fusion. Cell 92, 759–772.

West M, Zurek N, Hoenger A, Voeltz GK (2011). A 3D analysis of yeast ER structure reveals how ER domains are organized by membrane curvature. J Cell Biol 193, 333–346.

Zink S, Wenzel D, Wurm Ca, Schmitt HD (2009). A link between ER tethering and COP-I vesicle uncoating. Dev Cell 17, 403–416.

Zurek N, Sparks L, Voeltz G (2011). Reticulon short hairpin transmembrane domains are used to shape ER tubules. Traffic 12, 28–41.